Nanostructures

International Edition: DOI: 10.1002/anie.201501237
German Edition: DOI: 10.1002/ange.201501237

Cobalt Phosphide Nanowires: Efficient Nanostructures for Fluorescence Sensing of Biomolecules and Photocatalytic Evolution of Dihydrogen from Water under Visible Light**

*Jingqi Tian, Ningyan Cheng, Qian Liu, Wei Xing, and Xuping Sun**

Abstract: *The detection of specific DNA sequences plays an important role in the identification of disease-causing pathogens and genetic diseases, and photochemical water splitting offers a promising avenue to sustainable, environmentally friendly hydrogen production. Cobalt–phosphorus nanowires (CoP NWs) show a high fluorescence quenching ability and different affinity toward single- versus double-stranded DNA. Based on this result, the utilization of CoP NWs as fluorescent DNA nanosensors with a detection limit of 100 pM and a selectivity down to single-base mismatch was demonstrated. The use of a thrombin-specific DNA aptamer also enabled the selective detection of thrombin. The photoinduced electron transfer from the excited dye that labels the oligonucleotide probe to the CoP semiconductor led to efficient fluorescence quenching, and largely enhanced the photocatalytic evolution of hydrogen from water under visible light.*

The sequence-specific detection of DNA sequences that are associated with genetic and pathogenic diseases is of particular importance in molecular diagnostics.[1] Homogeneous assays based on fluorescence resonance energy transfer (FRET) or contact quenching are becoming increasingly popular because of their inherent advantages such as convenience of operation, rapid binding kinetics, and ease of automation.[2] Although such assays are widely used for many applications, they require the labelling of the probes at both ends with specific dyes that suffer from low overall synthetic yield and are not cost-effective.[3] In addition, both dyes must be carefully chosen to ensure efficient FRET or quenching. These issues can be solved by using a nanoquencher that is capable of quenching dyes with different emission frequencies,[4] and indeed, many nanostructures have been developed as efficient nanoquenchers for fluorimetric DNA detection, including Au nanoparticles,[5] carbon nanotubes (CNTs) and nanoparticles (CNPs),[6] graphene oxide (GO),[7] conjugation polymer nanostructures,[8] and MoS_2 nanosheets.[9]

The depletion of fossil fuels and increased environmental concerns have created an urgent demand for clean alternative energy sources.[10] Hydrogen is considered an ideal clean fuel for future energy applications.[11] Photochemical water splitting harvests natural solar energy as the driving force to split water and thus offers a promising strategy for cost-effective and environmentally friendly hydrogen production.[12] Recent studies have shown that CoP is capable of electrochemically catalyzing the hydrogen evolution reaction with high efficiency.[13] To the best of our knowledge, however, the use of CoP for biosensing and photocatalytic hydrogen generation remains unexplored. Here we describe the first use of CoP nanowires (CoP NWs) in fluorescent biosensing and photocatalytic hydrogen evolution. Their interesting versatility makes them strong candidates for multiple applications.

CoP NWs were obtained from the precursor $Co(CO_3)_{0.5}(OH)\cdot 0.11\,H_2O$[14] using an established phosphidation at low temperature.[13a–c] Figure 1A shows the X-ray diffraction (XRD) patterns of the precursor (curve a) and the phosphidated product (curve b). The diffraction peaks for the precursor can be assigned to orthorhombic $Co(CO_3)_{0.5}(OH)\cdot 0.11H_2O$ (JCPDS No. 48-0083),[14] while only peaks corresponding to orthorhombic CoP are observed (JCPDS No. 29-0497)[15] after the phosphidation. Figure 1B shows the low-magnification scanning electron microscopy (SEM) image of the precursor, indicating that it consists of a large amount of 1D nanostructures that are about several micrometers long. The high-magnification SEM images (insets) show that these nanowires have diameters ranging from 20 to 30 nm and that they still preserve their 1D morphology and sizes after phosphidation (Figure 1C). The energy-dispersive X-ray (EDX) spectrum for the resulting nanowires (Figure S1A) verifies the 1:1 atomic ratio of Co to P. The transmission electron microscopy (TEM) images of the $Co(CO_3)_{0.5}(OH)\cdot 0.11H_2O$ NWs (Figure 1D) and CoP NWs (Figure 1E) demonstrate that the smooth surface of $Co(CO_3)_{0.5}(OH)\cdot 0.11H_2O$ becomes rough after phosphidation. The high-resolution TEM (HRTEM) image taken from the

[*] Dr. J. Tian, N. Cheng, Q. Liu, Prof. X. Sun
State Key Laboratory of Electroanalytical Chemistry, Changchun Institute of Applied Chemistry, Chinese Academy of Sciences
Changchun 130022, Jilin (China)
E-mail: sunxp@ciac.ac.cn
Dr. J. Tian, N. Cheng
University of the Chinese Academy of Sciences
Beijing 100049 (China)
Prof. X. Sun
Chemistry Department & Center of Excellence for Advanced Materials Research, King Abdulaziz University
Jeddah 21589 (Saudi Arabia)
Prof. W. Xing
Laboratory of Advanced Power Sources, Changchun Institute of Applied Chemistry, Chinese Academy of Sciences
Changchun 130022, Jilin (China)

[**] This work was supported by the National Natural Science Foundation of China (No. 21175129), the National Basic Research Program of China (No. 2011CB935800), and the "Strategic Priority Research Program " of the Chinese Academy of Sciences (No. XDA09030104).

Supporting information for this article is available on the WWW under http://dx.doi.org/10.1002/anie.201501237.

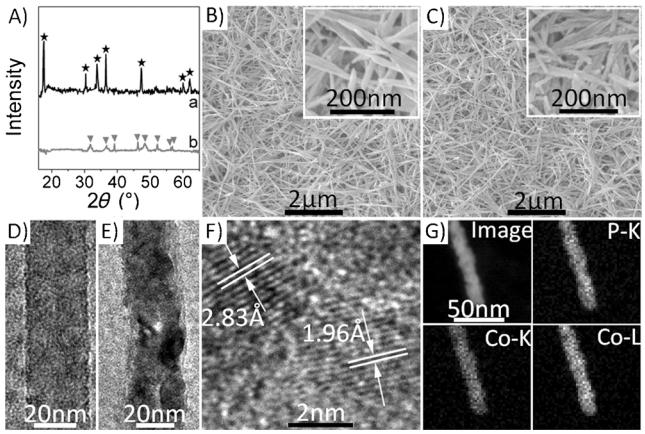

Figure 1. A) XRD patterns of $Co(CO_3)_{0.5}(OH)\cdot 0.11\,H_2O$ (curve a) and its phosphidated product (curve b). SEM images of B) $Co(CO_3)_{0.5}(OH)\cdot 0.11\,H_2O$ and C) the phosphidated product. TEM images of a single D) $Co(CO_3)_{0.5}(OH)\cdot 0.11\,H_2O$ NW and E) CoP NW. F) HRTEM image taken from the CoP NW. G) STEM image and the corresponding EDX elemental mapping images of P and Co for CoP NWs.

CoP NWs (Figure 1 F) shows well-resolved lattice fringes with interplanar distances of 2.83 and 1.96 Å indexed to the (011) and (112) planes of CoP, respectively. The diffraction rings in the selected area electron diffraction (SAED) pattern (Figure S1B) recorded from the CoP NWs can be identified as the (011), (111), (202), (103), and (301) planes of orthorhombic CoP.[15] The scanning TEM (STEM) image and the corresponding EDX elemental mapping images of P and Co for CoP NWs (Figure 1 G) further show that both elements, phosphorus and cobalt, are uniformly distributed in the whole nanowire.

We next chose an oligonucleotide sequence associated with human immunodeficiency virus (HIV), labelled at one end with a fluorescein-based dye (FAM) as the probe (P_{HIV}) for demonstration use. The EDX elemental mapping images of P, Co, and N for the P_{HIV}/CoP hybrid suggest the uniform distribution of these elements along the nanowire (Figure S2), thus providing clear evidence for the attachment of P_{HIV} to the CoP NWs. The zeta potential of the CoP NWs was about −13.7 mV, thus indicating that there are some electrostatic repulsion interactions between the negatively charged CoP NWs and the negatively charged backbone of P_{HIV}. So the adsorption of P_{HIV} on CoP should be driven by other interactions, which is confirmed by the corresponding X-ray photoelectron spectroscopy (XPS) data of CoP and the P_{HIV}/CoP hybrid. Compared to CoP, the P_{HIV}/CoP hybrid shows additional peaks of C and N (Figure S3A and S3B) and the binding energy (BE) at 779.1 eV in the Co(2p) region for CoP[16] is positively shifted to 779.5 eV (Figure S3C and S3D). Meanwhile, the P_{HIV}/CoP hybrid exhibits a negative shift of the BEs in the N(1s) region, including a pyrrolic N (400.3 eV), an amino N (399.3 eV), and a pyridinic N (398.4 eV), compared with the BEs for P_{HIV} (400.4 eV, 399.5 eV and 398.8 eV),[17] as shown in Figure S3E and S3F. The significant difference in electronegativity between metal and nonmetal elements favors electron transfer through noncovalent interactions from the donor to acceptor.[18] P_{HIV} is rich with free nucleobases and the great difference in electronegativity between Co and N causes electron transfer from Co to N, thus leading to a positive shift of the BE of Co and the negative shift of the BEs of N. Such noncovalent interactions should be stronger than the electrostatic repulsions between P_{HIV} and CoP and are thus responsible for the efficient adsorption of P_{HIV} on CoP. Such adsorption brings FAM into close proximity to the CoP surface, which could lead to fluorescence quenching.[5–9] When P_{HIV} is hybridized with T_1, its complementary strand, however, CoP should have weak or no affinity toward the resulting double-stranded (dsDNA) because of the absence of unpaired nucleobases and the rigid conformation of dsDNA, thus leading to the retention of the fluorescence. It is expected that this sensing principle can also be used for the detection of protein-like thrombin (TB) by utilizing its aptamer labelled with dye (TA) as the fluorescent probe, because the presence of TB results in the change of the TA conformation to quadruplex to form a quadruplex–TB complex, thereby weakening the affinity of CoP toward TA.[19] Figure 2 illustrates the sensing mechanism for biomolecule detection based on the retention of the fluorescence.

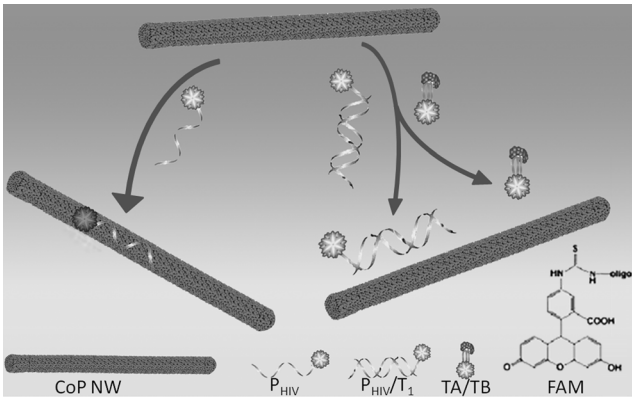

Figure 2. A schematic diagram to illustrate the sensing mechanism for biomolecule detection based on fluorescence retention.

The fluorescence emission spectra of P_{HIV} under different conditions are shown in Figure 3 A. In the buffer, P_{HIV} exhibits strong fluorescence emission arising from FAM (curve a). The incubation of P_{HIV} with a large excess of T_1 causes their efficient hybridization to form a P_{HIV}/T_1 duplex, which retains the fluorescence of P_{HIV} (curve b). However, CoP influences the fluorescence intensity of P_{HIV} and P_{HIV}/T_1. With the presence of CoP, the fluorescence of P_{HIV}/T_1 was slightly quenched (about 16%, curve c), while the fluorescence of P_{HIV} was largely quenched (about 65%, curve d). Note that the CoP NWs themselves have no fluorescence (curve e). We studied the quenching kinetics of CoP toward P_{HIV} and P_{HIV}/T_1 and found that only 7 min were required for efficient quenching (inset in Figure 3 A). All these observations confirmed the strong fluorescence quenching ability, the different affinity toward single-stranded DNA (ssDNA) versus dsDNA, and the fast quenching kinetics of CoP NWs, thus providing an ideal detection method for fluorescent DNA.

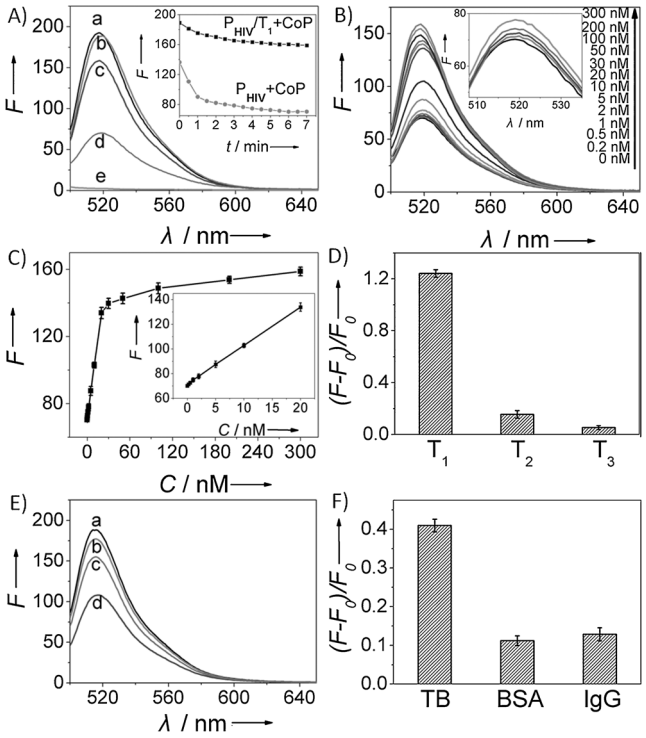

Figure 3. A) Fluorescence spectra of P_{HIV} (50 nM) under different conditions: a) P_{HIV}; b) $P_{HIV}+T_1$ (300 nM); c) $P_{HIV}+T_1$ (300 nM) + CoP NWs; d) P_{HIV} + CoP NWs; e) CoP NWs. Inset: kinetic study of the fluorescence change of P_{HIV} and P_{HIV}/T_1 in the presence of CoP. B) Fluorescence spectra of P_{HIV} (50 nM) + T_1 at different concentrations in the presence of CoP (inset: amplification of the concentration range from 0 to 2 nM). C) Corresponding calibration curve (inset: amplification of the low-concentration range). D) Fluorescence intensity changes $[(F-F_0)/F_0]$ of P_{HIV} (50 nM) + CoP NWs in the presence of T_1 (300 nM), T_2 (300 nM), or T_3 (300 nM) (F_0 and F are the fluorescence intensities of P_{HIV} + CoP NWs in the absence and presence of complementary strands, respectively). E) Fluorescence spectra of TA (20 nM) under different conditions: a) TA; b) TA + TB (100 nM); c) TA + TB (100 nM) + CoP NWs; d) TA + CoP NWs. F) Fluorescence intensity changes $[(F-F_0)/F_0]$ of TA (20 nM) + CoP NWs in the presence of TB (100 nM), BSA (100 nM), or IgG (100 nM). Excitation was at 480 nm and the emission was monitored at 518 nm. All measurements were done in Tris-HCl buffer containing 100 nM NaCl, 5 mM KCl, and 5 mM $MgCl_2$ (pH: 7.4).

We probed the sensitivity of this nanosensor by collecting the fluorescence emission spectra of $P_{HIV}+T_1$ with T_1 at different concentrations in the presence of CoP. An increased concentration of T_1 led to an intensified retention of the fluorescence intensity (Figure 3B). On the basis of the derived calibration curve (Figure 3C), the CoP sensor shows a linear range from 0.2 to 20 nM. The detection limit (three times the standard deviation in the blank solution) is 100 pM, which is lower than that of most reported nanoquenchers listed in Table S1. It is also important to mention that our nanosensor only needs 14 min to complete the whole "mix-and-detect" process. The nonlinear character of the calibration curve over the entire concentration range is probably due to that the increased concentration of T_1, which results in a gradually more hybridization events near the CoP surface.[20] This nanosensor also shows the ability to discriminate the complementary strand and the single-base mismatched one. Figure 3D shows fluorescence intensity changes $(F-F_0)/F_0$ of $P_{HIV}+CoP$ with the presence of T_1, the single-base mismatched strand T_2, or the noncomplementary strand T_3. The value for T_2 is about 15% of the value for T_1, but the change in fluorescence intensity that occurs for T_3 is quite small. These observations demonstrate that the CoP nanosensor has a high selectivity down to a single-base mismatch with good reproducibility.

We further demonstrate the generality of this nanosensor for protein detection using TB as a model system. Figure 3E shows the fluorescence spectra of TA under different conditions. CoP NWs led to about 42% quenching of the fluorescence of the dye. In sharp contrast, in the presence of TB, CoP NWs only resulted in about 17% quenching. To assess the specificity of this fluorescent nanosensor for TB, two other proteins, including bovine serum albumin (BSA) and human IgG, were examined. Both proteins failed to cause a distinct change in the fluorescence at an equal concentration to TB (Figure 3F). All these results prove that our CoP nanosensor can be used for the selective detection of TB. Thus, the CoP NWs are effective in probing biomolecular interactions. Results from both SEM and TEM indicate that the CoP NWs maintain their initial morphology after the sensing cycle (Figure S4), thus implying the superior morphological stability.

Figure 4A presents the photocurrent responses of fluorine-doped tin oxide (FTO) coated glass slides modified with CoP NWs and P_{HIV}/CoP hybrids under visible light at a bias of 0.0 V. An anodic photocurrent is observed for CoP NWs upon illumination (curve a), showing that the photogenerated electrons move to the FTO electrode because of the n-type nature of CoP. Compared to CoP NWs, the FTO modified with the P_{HIV}/CoP hybrid shows an enhanced photocurrent (curve b), implying the transfer of photoexcited electrons from FAM to CoP. Based on the UV-Vis absorption spectrum of the CoP NWs (Figure 4B), we plotted the square of the absorption energy (αhv, where α is the absorbance) against the photoenergy (hv), as shown in Figure 4C. The band gap was determined to be 1.72 eV by extrapolating the linear fitting, consistent with the reported value of 1.71 eV.[21] The positive slope of the Mott–Schottky (MS) plot also confirms CoP to be a n-type semiconductor (Figure 4D). The flat-band potential for CoP was −0.47 V versus Ag/AgCl (Figure 4E). Because of the small difference between the flat-band potential and the lower conduction band (CB) edge,[22] the CB potential for CoP was roughly estimated to be −0.27 V versus NHE, which is more negative than the energy level for H_2 evolution (−0.059 V vs. NHE, pH 1), implying the potential application of CoP toward photocatalytic hydrogen generation. Additionally, the lowest unoccupied molecular orbital (LUMO) level of FAM is also more negative than the level of the CB edge of CoP,[23] which drives electron injection from the excited FAM to CoP through photoinduced electron transfer (PET),[24] and as a result, quenching of the fluorescence occurs. Note that although P_{HIV}/CoP shows a significantly decreased fluorescence intensity, the addition of T_1 leads to a highly efficient recovery of the fluorescence with an intensity comparable to that for P_{HIV}/T_1+CoP (Figure S5),

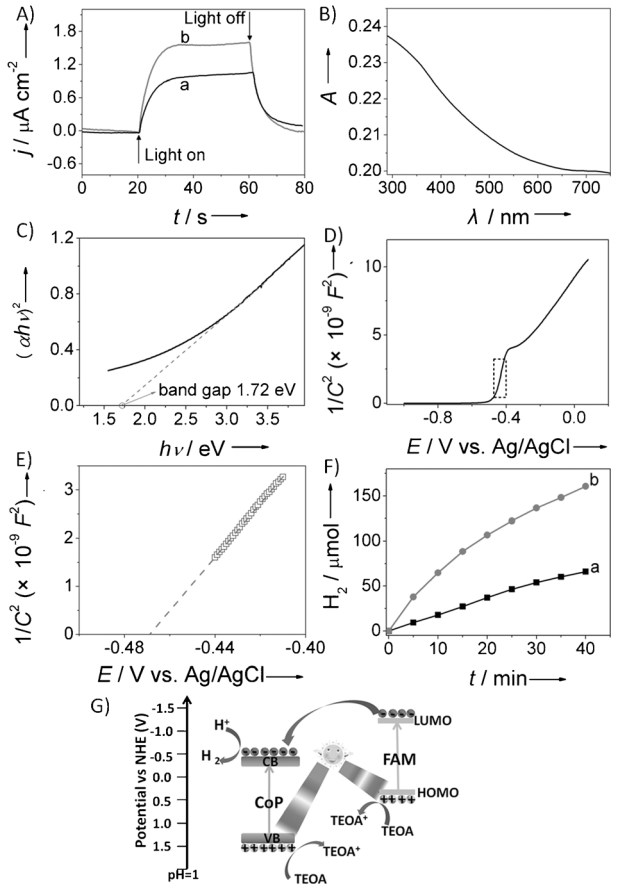

Figure 4. A) Photocurrent of a) CoP NWs and b) P_{HIV}/CoP hybrid measured at a bias of 0.0 V against the Ag/AgCl reference electrode under visible light illumination ($\lambda > 420$ nm) (electrolyte: H_2SO_4, pH 1.0). B) UV-Vis absorption spectrum of CoP NWs. C) Plot of $(\alpha h\nu)^2$ against photon energy ($h\nu$) for CoP NWs. D) Mott–Schottky plot of CoP NWs. E) Amplification of the dashed rectangle region in (D). F) Amount of H_2 generated as a function of irradiation time with a) CoP and b) P_{HIV}/CoP hybrid under visible light ($\lambda > 420$ nm). G) Energy level diagram to illustrate photocatalytic hydrogen evolution using P_{HIV}/CoP hybrid as photocatalyst.

excluding the involvement of photo-oxidation of P_{HIV} in the fluorescence sensing.

We further explored the application of both the CoP NWs and the P_{HIV}/CoP hybrids as photocatalysts for the photochemical hydrogen evolution under visible light using triethanolamine (TEOA) as a sacrificial agent. Figure 4F shows the reaction time courses for the evolution of H_2. The amount of evolving H_2 increased continuously and irradiation for 40 min produced 66.1 μmol H_2 using CoP (curve a). In contrast, a total amount of 160.7 μmol H_2 was produced using the P_{HIV}/CoP hybrid within the same time (curve b). These results show that the attachment of dye-labelled probes to CoP largely improves its photocatalytic hydrogen-evolution ability, which can be attributed to the PET from the LUMO of the excited dye to the CB of CoP, which allows a more efficient electron accumulation on the CoP surface for the reduction of protons. Both the holes in the valence band (VB) of CoP and the oxidized dye accept electrons from TEOA at the same time, thus leading to an efficient charge separation. Figure 4G shows an energy level diagram that illustrates the photocatalytic H_2 generation from water using the P_{HIV}/CoP hybrid as the photocatalyst. Table S2 lists the comparison of the hydrogen evolution rate of the P_{HIV}/CoP hybrid with other reported photocatalysts, suggesting that P_{HIV}/CoP is efficient for the photocatalytic hydrogen evolution. It is believed that the depletion of electrons on the CoP for proton reduction also accelerates the PET process, which leads to an enhanced sensing speed and performance.

We also prepared CoP nanoparticles (CoP NPs, Figure S6) and examined their ability for quenching and photocatalytic H_2 generation. CoP NPs can also quench the fluorescence of P_{HIV}, but with decreased quenching efficiency (53%), as shown in Figure S7. In addition, they also exhibits much inferior catalytic activity compared to to CoP NWs, and the hybrid of CoP NPs with P_{HIV} only produces a total amount of 66.7 μmol H_2, which is much lower than that generated by the hybrid based on CoP NWs (160.7 μmol) within the same period (Figure S8). All these observations suggest that the morphology of CoP has a strong influence on its properties and that the one-dimensional nanostructure (wires) is superior in fluorescence quenching and photocatalytic H_2 evolution over its zero-dimensional counterpart (particles), thus implying more efficient charge separation and electron transfer.

In conclusion, we have used the differential adsorption of ssDNA and dsDNA by CoP NWs to design a simple and rapid fluorescence assay for nucleic acids and proteins. Beyond their use for biosensing, the nanowires have also been utilized for the photocatalytic evolution of hydrogen from water under visible light with largely enhanced activity after attachment of dye-labelled oligonucleotide probes. All these remarkable features, along with the scale-up synthesis, may open new avenues to develop cost-effective transition-metal phosphides (TMPs) for fluorescence sensing and photocatalytic applications. The good electrical conductivity of TMPs[25] and the easy growth of their 1D nanostructures on current collectors[13b,26] would also offer interesting nanoarray electrodes for electrochemical sensing.

Keywords: biomolecules · fluorescence sensing · hydrogen evolution · CoP nanowires · photocatalysis

How to cite: *Angew. Chem. Int. Ed.* **2015**, *54*, 5493–5497
Angew. Chem. **2015**, *127*, 5583–5587

[1] a) A. J. Schafer, J. R. Hawkins, *Nat. Biotechnol.* **1998**, *16*, 33–39; b) C. Debouck, P. N. Goodfellow, *Nat. Genet.* **1999**, *21*, 48–50; c) R. Favis, J. P. Day, N. P. Gerry, C. Phelan, S. Narod, F. Barany, *Nat. Biotechnol.* **2000**, *18*, 561–564; d) V. Gubala, L. F. Harris, A. J. Ricco, M. Tan, D. E. Williams, *Anal. Chem.* **2012**, *84*, 487–515; e) L. Esfandiari, M. Lorenzini, G. Kocharyan, H. G. Monbouquette, J. J. Schmidt, *Anal. Chem.* **2014**, *86*, 9638–9643.

[2] a) J. L. Bock, *Am. J. Clin. Pathol.* **2000**, *113*, 628–646; b) B. Liu, G. C. Bazan, *Chem. Mater.* **2004**, *16*, 4467–4476; c) K. Wang, Z. Tang, C. Yang, Y. Kim, X. Fang, W. Li, Y. Wu, C. D. Medley, Z. Cao, J. Li, P. Colon, H. Lin, W. Tan, *Angew. Chem. Int. Ed.* **2009**, *48*, 856–870; *Angew. Chem.* **2009**, *121*, 870–885.

[3] A. P. Misra, P. Kumar, K. C. Gupta, *Anal. Biochem.* **2007**, *364*, 86–88.

[4] P. C. Ray, G. K. Darbha, A. Ray, J. Walker, W. Hardy, *Plasmonics* **2007**, *2*, 173 – 183.
[5] a) H. Li, L. Rothberg, *Proc. Natl. Acad. Sci. USA* **2004**, *101*, 14036 – 14039; b) H. Li, L. J. Rothberg, *Anal. Chem.* **2004**, *76*, 5414 – 5417.
[6] a) R. Yang, J. Jin, Y. Chen, N. Shao, H. Kang, Z. Xiao, Z. Tang, Y. Wu, Z. Zhu, W. Tan, *J. Am. Chem. Soc.* **2008**, *130*, 8351 – 8358; b) H. Li, J. Tian, L. Wang, Y. Zhang, X. Sun, *Chem. Commun.* **2011**, *47*, 961 – 963.
[7] C. Lu, H. Yang, C. Zhu, X. Chen, G. Chen, *Angew. Chem. Int. Ed.* **2009**, *48*, 4785 – 4787; *Angew. Chem.* **2009**, *121*, 4879 – 4881.
[8] a) L. Wang, Y. Zhang, J. Tian, H. Li, X. Sun, *Nucleic Acids Res.* **2011**, *39*, e37 – e42; b) S. Liu, L. Wang, Y. Luo, J. Tian, H. Li, X. Sun, *Nanoscale* **2011**, *3*, 967 – 969; c) W. Qiang, W. Li, X. Li, X. Chen, D. Xu, *Chem. Sci.* **2014**, *5*, 3018 – 3024.
[9] C. Zhu, Z. Zeng, H. Li, F. Li, C. Fan, H. Zhang, *J. Am. Chem. Soc.* **2013**, *135*, 5998 – 6001.
[10] a) M. Graetzel, *Acc. Chem. Res.* **1981**, *14*, 376 – 384; b) A. J. Bard, M. A. Fox, *Acc. Chem. Res.* **1995**, *28*, 141 – 145.
[11] a) T. J. Meyer, *Acc. Chem. Res.* **1989**, *22*, 163 – 170; b) J. A. Turner, *Science* **2004**, *305*, 972 – 974.
[12] a) A. Kudo, Y. Misekia, *Chem. Soc. Rev.* **2009**, *38*, 253 – 278; b) J. Ran, J. Zhang, J. Yu, M. Jaroniec, S. Z. Qiao, *Chem. Soc. Rev.* **2014**, *43*, 7787 – 7812.
[13] a) Q. Liu, J. Tian, W. Cui, P. Jiang, N. Cheng, A. M. Asiri, X. Sun, *Angew. Chem. Int. Ed.* **2014**, *53*, 6710 – 6714; *Angew. Chem.* **2014**, *126*, 6828 – 6832; b) J. Tian, Q. Liu, A. M. Asiri, X. Sun, *J. Am. Chem. Soc.* **2014**, *136*, 7587 – 7590; c) Z. Pu, Q. Liu, P. Jiang, A. M. Asiri, A. Y. Obaid, X. Sun, *Chem. Mater.* **2014**, *26*, 4326 – 4329; d) E. J. Popczun, C. G. Read, C. W. Roske, S. Lewis, R. E. Schaak, *Angew. Chem. Int. Ed.* **2014**, *53*, 5427 – 5430; *Angew. Chem.* **2014**, *126*, 5531 – 5534; e) Z. Huang, Z. Chen, Z. Chen, C. Lv, M. G. Humphrey, C. Zhang, *Nano Energy* **2014**, *9*, 373 – 382.
[14] B. Wang, T. Zhu, H. Wu, R. Xu, J. Chen, X. Lou, *Nanoscale* **2012**, *4*, 2145 – 2149.
[15] Y. Li, M. A. Malik, P. O'Brien, *J. Am. Chem. Soc.* **2005**, *127*, 16020 – 16021.
[16] A. P. Grosvenor, S. D. Wik, R. G. Cavell, A. Mar, *Inorg. Chem.* **2005**, *44*, 8988 – 8998.
[17] C. Zhang, R. Hao, H. Liao, Y. Hou, *Nano Energy* **2013**, *2*, 88 – 97.
[18] a) G. Kladnik, D. Cveko, A. Batra, M. Dell'Angela, A. Cossaro, M. Kamenetska, L. Venkataraman, A. Morgante, *J. Phys. Chem. C* **2013**, *117*, 16477 – 16482; b) *Characterization of Biomaterials* (Eds.: A. Bandyopadhyay, S. Bose), Elsevier, Waltham, MA, **2013**.
[19] Y. Zhang, X. Sun, *Chem. Commun.* **2011**, *47*, 3927 – 3929.
[20] P. Alonso-Cristobal, P. Vilela, A. El-Sagheer, E. Lopez-Cabarcos, T. Brown, O. L. Muskens, J. Rubio-Retama, A. G. Kanaras, *ACS Appl. Mater. Interfaces* **2015**, DOI: 10.1021/am507591u.
[21] W. Maneeprakorn, M. A. Malik, P. O'Brien, *J. Mater. Chem.* **2010**, *20*, 2329 – 2335.
[22] a) A. Ishikawa, T. Takata, J. N. Kondo, M. Hara, H. Kobayashi, K. Domen, *J. Am. Chem. Soc.* **2002**, *124*, 13547 – 13553; b) J. Lv, T. Kako, Z. Li, Z. Zou, J. Ye, *J. Phys. Chem. C* **2010**, *114*, 6157 – 6162.
[23] a) Q. Wang, W. Wang, J. Lei, N. Xu, F. Gao, H. Ju, *Anal. Chem.* **2013**, *85*, 12182 – 12188; b) Y. Wang, J. Hong, W. Zhang, R. Xu, *Catal. Sci. Technol.* **2013**, *3*, 1703 – 1711; c) X. Wang, K. Maeda, A. Thomas, K. Takanabe, G. Xin, J. M. Carlsson, K. Domen, M. Antonietti, *Nat. Mater.* **2009**, *8*, 76 – 80.
[24] a) B. O'Regan, M. A. Grätzel, *Nature* **1991**, *353*, 737 – 740; b) A. P. de Silva, H. Q. Gunaratne, T. Gunnlaugsson, A. J. Huxley, C. P. McCoy, J. T. Rademacher, T. E. Rice, *Chem. Rev.* **1997**, *97*, 1515 – 1566; c) R. Lincoln, L. E. Greene, K. Krumova, Z. Ding, G. Cosa, *J. Phys. Chem. A* **2014**, *118*, 10622 – 10630.
[25] S. T. Oyama, T. Gott, H. Zhao, Y. K. Lee, *Catal. Today* **2009**, *143*, 94 – 107.
[26] a) J. Tian, Q. Liu, N. Cheng, A. M. Asiri, X. Sun, *Angew. Chem. Int. Ed.* **2014**, *53*, 9577 – 9581; *Angew. Chem.* **2014**, *126*, 9731 – 9735; b) P. Jiang, Q. Liu, Y. Liang, J. Tian, A. M. Asiri, X. Sun, *Angew. Chem. Int. Ed.* **2014**, *53*, 12855 – 12859; *Angew. Chem.* **2014**, *126*, 13069 – 13073; c) Y. Liang, Q. Liu, A. M. Asiri, X. Sun, Y. Luo, *ACS Catal.* **2014**, *4*, 4065 – 4069.

Received: February 9, 2015
Published online: February 26, 2015

